Capacitive RF discharges modelled by particle-in-cell Monte Carlo simulation. I. Analysis of numerical techniques

1993 Plasma Sources Sci. Technol. 2 261

(http://iopscience.iop.org/0963-0252/2/4/006)

Plasma Sources Sci. Technol. 2(1993) 261–272. Printed in the UK

Capacitive RF discharges modelled by particle-in-cell Monte Carlo simulation. I: analysis of numerical techniques

V Vahedi†, G DiPeso‡, C K Birdsall†, M A Lieberman†, and T D Rognlien‡

†Department of Electrical Engineering and Computer Science, University of California, Berkeley, CA 94720, USA
‡Lawrence Livermore National Laboratory, Livermore, CA 94550, USA

Received 25 February 1993, in final form 11 July 1993

Abstract. Particle-in-cell Monte Carlo simulation has become a very effective tool in exploring processing plasmas and in particular capacitive RF discharges. We describe the conventional particle-in-cell (PIC) simulation and its limitations in terms of computational efficiency, review the implicit subcycling methods used to improve computational efficiency for many problems, and analyse conventional and implicit subcycling PIC simulation performances on an RF discharge model. Implementation of the implicit subcycling scheme in our bounded one-dimensional electrostatic code, PDP1, resulted in an order of magnitude reduction in the simulation run time when the accuracy conditions were satisfied.

1. Introduction

The RF capacitive glow discharges and other plasmas are extensively used in the microelectronics industry. In recent years, computer modelling and simulation have emerged to complement laboratory experiments [1–5] and analytic models [6–8] as effective and important tools in increasing general understanding of processing plasmas. Simulations especially have proven very useful in providing insights into some discharge parameters that are not easily accessible to laboratory measuring devices.

An abnormally low electron energy was experimentally measured by Godyak *et al* [1] in argon RF discharges at 13.56 MHz, and explained as the combined effect of stochastic electron heating and the Ramsauer effect [1]. Electrons at low energies are believed to be created through inelastic collisions (such as ionization) between high-energy electrons and neutral particles [2]. The low-energy group, with its temperature close to the Ramsauer minimum, has a very low electron–neutral collision cross section; this results in a low e–n collision frequency ν_{en} for this class of electrons. Thus, these electrons oscillate almost collisionlessly, unable to gain energy either from the low electric field in the plasma bulk (ohmically) or from the oscillating RF sheaths (stochastically). Although most of the low-energy electrons are trapped in the bulk by the DC ambipolar potential barrier, some overcome the barrier and diffuse out towards the plasma–sheath interface, where they can be stochastically heated by the oscillating sheaths to re-populate the high-energy electron group. The high-energy electrons are then either lost to the walls or lost to the low-energy group through inelastic collisions as discussed before. Thus, the overall electron energy distribution in the system appears like the sum of two Maxwellian energy distributions. Since these discharges are inherently complex, there has been a considerable effort to develop self-consistent kinetic models from first principles without making any assumptions about the distribution functions. Self-consistent fluid equations have been used by Graves and Jensen [9] Boeuf [10], Gogolides *et al* [11] and Meyyappan *et al* [12] to study the structural features of RF and DC glows. However, these models assume a certain distribution function (typically Maxwellian) for the particles.

Particle-in-cell (PIC) simulation is a well-established tool for kinetic modelling in plasma physics [13] as well as in solid state physics and astrophysics [14]. The basic idea of PIC simulation is to allow thousands of computer-simulated particles (super-particles) to represent many more (10^8–$10^{12}\,cm^{-3}$) real particles in a laboratory device. In plasmas, we are often interested in collective effects; such a representation is possible if we allow the particles to interact with electromagnetic fields calculated on a numerical grid. Particle–particle inter-

0963-0252/93/040261+12 $07.50

actions within a grid spacing, such as electron–ion Coulomb collisions, can also be modelled with computer-simulated particles and included in a PIC simulation [14, 15].

In order to use particle-in-cell (PIC) simulation codes for modelling collisional plasmas and self-sustained discharges, it is necessary to add interactions between charged and neutral particles. In conventional Monte Carlo schemes [16–21], the time or distance between collisions for each particle is calculated using random numbers. This procedure allows for efficient algorithms, especially when the null collision method is also used [21, 22], but is not compatible with PIC simulations where the charged particle trajectories are all integrated simultaneously in time. A Monte Carlo collision (MCC) package, including the null collision method [21, 22], has been developed [23, 24], as an addition to the usual PIC charged particle scheme, as shown in figure 1. Birdsall [24], Vender [25], Surendra *et al* [26], Vahedi *et al* [27], Alves *et al* [28] and Turner *et al* [29] have used particle-in-cell Monte Carlo (PIC-MCC) techniques to study RF discharges, showing excellent agreement between PIC simulation results and analytic predictions. It should be noted that hybrid (fluid–particle) Monte Carlo modelling of weakly ionized plasmas by Boeuf and Pitchford [30], Sato and Tagashira [31] and Sommerer and Kushner [32] has also been successful.

Birdsall [24] presented a historical overview of PIC-MCC as used in simulating plasma assisted materials processing (PAMP) devices and fusion plasmas. Here we will specialize in PIC-MCC simulations of bounded capacitive RF discharges, which exhibit a wide range of time scales. In planar RF discharges, a plasma is bounded between two parallel plates and is driven by an external source. The drive frequency ω_0 (typically 13.56 MHz) is normally at least an order of magnitude smaller than the electron plasma frequency ω_{pe}. This allows the electrons to respond to the instantaneous applied field. The ions are much heavier than the electrons and respond only to the time-averaged fields in the system, typically with $\omega_{pi} < \omega_0$. In the high-pressure regime, where the mean free path for ion–neutral collisions becomes much smaller than the system length, the ion loss is ambipolar-diffusion-limited. This makes the ion transit time scale the longest time scale in the system. The discharge typically equilibrates over many ion transit time scales, which is much longer than the RF cycle $2\pi/\omega_0$. Assuming that fast plasma phenomena (on the plasma frequency time scales) are not significant in the RF discharge physics, the highest frequency that must be resolved for accurate modelling of the RF physics is the RF driving frequency ω_0.

Unfortunately the stability condition for the conventional explicit PIC requires the resolution of the electron plasma frequency ω_{pe}. That is, if the simulation time step size Δt is such that $\omega_{pe}\Delta t > 2$, numerical instabilities can occur [13]. Because $\omega_0 \leqslant \omega_{pe}$ the stability condition results in computational inefficiency by requiring a much smaller Δt for the numerics than would be required to observe the physics of interest with typical frequencies of the order of ω_0. Thus, we implement some optimizing algorithms, which result in an order of magnitude reduction in the simulation run time. These algorithms are incorporated into our bounded one-dimensional electrostatics code called PDP1 [24, 33], which was derived from Lawson's bounded PIC code PDW1 [34]. Lawson gives a thorough discussion of bounded one-dimensional plasma systems [34] for conventional explicit PIC simulations. Our PDP1 simulates a bounded one-dimensional plasma device with external sources and circuit elements as shown in figure 2. Various boundary conditions may be applied to the system [35]; the external circuit may be driven by a voltage or current source.

2. Background

Finite-difference methods for integrating an equation of the form

$$\partial_t u = f(u, t)$$

can be divided into two classes. One class is explicit methods, in which the value of u at time $t = n + 1$ is related only to the values of u and $f(\ )$ and time $t = n$ and before, for example

$$u^{n+1} = u^n + \Delta t f(u^n, n). \tag{1}$$

The other class is implicit methods, in which the value of u at time $t = n + 1$ is related to the values of u and

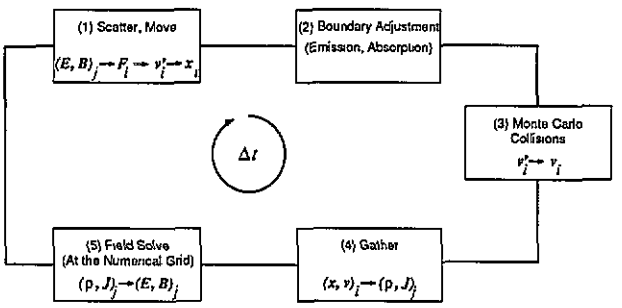

Figure 1. The flow chart for an explicit PIC scheme with addition of the Monte Carlo collision package, called PIC-MCC.

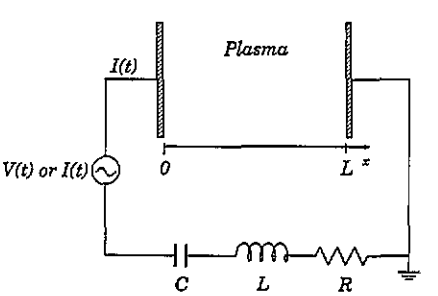

Figure 2. The flow chart for an explicit PIC scheme with addition of the Monte Carlo collision handler, called PIC-MCC.

$f(\ )$ at times $t = n + 1$, $t = n$ and before, for example

$$u^{n+1} = u^n + \frac{\Delta t}{2}\,[f(u^{n+1}, n+1) + f(u^n, n)]. \qquad (2)$$

The main advantage of explicit methods is that they are easy to program and the number of operations (multiplications) is low. However, there are also disadvantages, which, in some cases, outwiegh the advantages. Explicit methods are typically constrained by stability requirements, which place restrictions on the choice of time step. Implicit methods, on the other hand, are stable over a larger (if not all-encompassing) range of time steps. The stability of implicit methods is at the cost of more operations and more complicated algorithms. Sod [36] gives a more detailed discussion of these methods and the stability requirements for various explicit scheme. Birdsall and Langdon present detailed discussions for stability and accuracy of various explicit and implicit schemes used in particle-in-cell simulations.

In this paper, we describe the conventional explicit PIC simulation and its limitations in terms of computational efficiency, review an implicit method, which improves computational efficiency for many problems, and compare conventional and implicit PIC simulation performance for an RF discharge model. Because the MCC algorithm imposes less stringent constraints on temporal and spatial scales than the PIC scheme, the MCC package will be only briefly reviewed here. A more detailed discussion of MCC can be found in papers by Surendra *et al* [23], Birdsall [24] and Vahedi [33]. (In part II of this paper, we will compare the results obtained from PDP1 with published laboratory measurements obtained by Godyak *et al* [1, 2].)

3. Conventional bounded PIC-MCC

The boxes labelled (1), (4), and (5) in figure 1 constitute the conventional explicit PIC simulation scheme for periodic models; box (2) is added for bounded models. At the beginning of each time step, given the electromagnetic fields known on a numerical grid at a certain point in time, the force on each computer particle (super-particle) is calculated in order to advance the velocity and position of each super-particle with the same equations of motion that would be used for real particles. Because the fields are known only on the numerical grid, fields at the actual particle location are determined by interpolation. This step is called 'scatter'. In a bounded PIC scheme, after each particle position is advanced in time, the new location is tested to determine whether the particle has reached the boundaries. If so, depending on the type of boundary conditions imposed, the particle is absorbed, reflected, or absorbed emitting another particle (as in secondary electron emission). The locations and velocities of the particles that remain in the system are used to determine the charge and current density on the grid, again using interpolation. This step is called 'gather'. These quantities are then used as source terms in Maxwell's equations, along with the applied boundary conditions, to advance the electromagnetic fields at the end of the time step.

Note that in figure 1, after the particles are advanced by the fields, the particles can be operated on by the MCC package, box (3), which handles the charged–neutral and neutral–neutral particle collisions. Collision is assumed to take place at the current location of each particle. The collision is modelled with three velocity components. We take the neutral particles to have a Maxwellian velocity distribution and a uniform density. The model remains valid if the neutral density is a function of position and time. This scheme can also be extended to model Coulomb collisions.

Briefly, the null collision method postulates a fictitious collision such that, when its collision frequency is added to the total collision frequency, the 'new' total collision frequency becomes constant over the entire energy range. This gives the same collision probability for all particles, independent of the energy. Thus, instead of querying all simulation particles to determine whether a collision has occurred, a certain fraction of all particles may be picked at random and tested. This method has been shown [33] to reduce substantially the CPU time for MCC operations.

The MCC package used here models an argon discharge with electron–neutral elastic, excitation and ionization collisions as well as ion–neutral scattering and charge-exchange collisions. Figure 3 shows the electron–neutral cross sections in the model, which are the same as those used by Surendra *et al* [37]. Figure 4 shows the ion–neutral cross sections used in the model [38].

In the one-dimensional model of an RF discharge, we consider only one dimension in space but three dimensions in velocity. Furthermore, Maxwell's equations are reduced to Poisson's equation by assuming that only the electrostatic field is important. The electrostatic boundary conditions are determined by the applied RF voltage (or current) source and external circuit parameters. Particles that hit the conducting walls contribute to the surface charge densities. Time variations of these charge densities affect the current in the external circuit. By modelling discharge chemistry with the MCC package

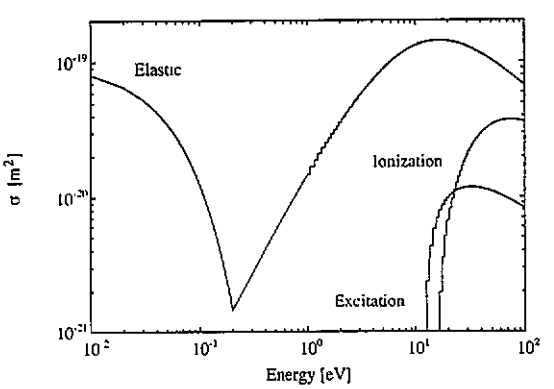

Figure 3. The argon electron–neutral cross sections used in this model.

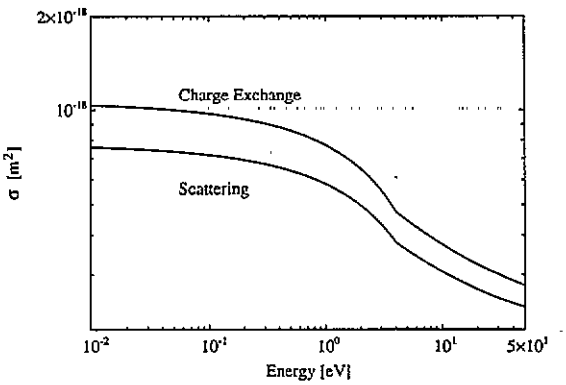

Figure 4. The argon ion–neutral cross sections used in this model.

and modelling external controls with the appropriate boundary conditions, developed by Verboncoeur *et al* [35], we have added some realism to our PIC simulations.

3.1. Timing of RF discharge simulations

In a typical one-dimensional PIC simulation, the number of particles is about two orders of magnitude larger than number of mesh points. Thus, most of the computational time is spent in the modules that deal with particle quantities (boxes (1)–(4) in figure 1). For example, in a normal simulation, 38% of the computational time is spent in the 'move' ('scatter') module (box (1)), followed by 29% in 'gather' (box (4)), 20% in 'boundary adjustment' (box (2)), 10% in 'MCC' (box (3)), and less than 1% in 'field solve' (box (5)). With the implementation of the null-collision algorithm, the time spent in the MCC module depends on the overall collision frequency. As the background gas pressure is raised, the percentage of the time spent in this module increases, but usually remains less than that spent in 'gather/scatter' modules. By assuming one-dimensional spatial variation and electrostatic fields, we have greatly simplified our simulation. Unfortunately, even with these simplifications, much GPU time is still spent before discharge equilibrium is reached because of the stability requirements in conventional PIC. For example, running a discharge simulation for one thousand RF cycles typically requires of the order of a million time steps. With 4×10^4 particles running at 10 μs per particle per Δt on a typical desk-top work-station, the run time is about 100 h (4 days). Later we show how to reduce this run time by a factor of two (using electron subcycling, see section 4), and by a factor of ten (using implicit subcycling, section 3.2).

3.2. Self-heating

Even if the code is stable, violating the accuracy conditions $\omega_{pe}\Delta t < 0.2$ and $\Delta x/\lambda_{De} < 1$ (where Δx is the numerical grid size and λ_{De} is the electron Debye length) can lead to more noise in the system [13]. In conventional particle simulations, numerical fluctuation in the system is inversely proportional to $(N_D + N_c)$ where N_D is the number of computer particles per Debye length λ_{De}, and N_c is the number of computer particles per cell [13]. This numerical noise over several plasma periods can increase the average kinetic energy of the particles. The time to double the average kinetic energy of the particles is known as the numerical heating time (or self-heating time [39]). If the run time of the simulation is a few plasma periods, this numerical heating can be tolerable. For RF discharge simulations, which usually require several hundred RF cycles to reach equilibrium (thousands of plasma cycles), this numerical heating can create substantial error in the electron temperature.

In an electropositive discharge, ions are created through ionization in the system and are lost through recombination at the electrodes. A simple overall power balance for the electrons in the system produces [7]

$$P_{el} \propto e n_s u_B \mathscr{E}_L \tag{3}$$

where P_{el} is the power density deposited into the electrons, n_s is the ion density at the sheath edge, $\mathscr{E}_L$ is the electron energy loss per ionization event, and $u_B = (kT_e/M)^{1/2}$ is taken to be the ion sound speed at the sheath edge in a single-temperature discharge. Note that $n_s \propto n$, where n is the average plasma density in the system. The ion loss rate u_B increases as the electron temperature is raised. It is clear from equation (3) that for a fixed power, as the electron temperature increases, the plasma density decreases. The conventional PIC simulation must then run with small enough grid spacing to resolve the electron Debye length λ_{De}, and use hundreds of thousands of particles to reduce the numerical noise and associated self-heating. This is why conventional particle simulation is considered numerically very expensive.

Self-heating can be decreased by reducing the numerical fluctuations on the scale of grid spacing (short-wavelength noise). These fluctuations are caused by a small non-uniform number of particles per cell and appear in the particle charge density terms ρ_s after the particles are weighted to the grid points. The overall charge density which serves as the source term in Poisson's equation is then

$$\rho = \sum_s \rho_s. \tag{4}$$

If the charge density ρ or the terms ρ_s are low-pass filtered in space before solving Poisson's equation, the short-wavelength noise in the electric field will be greatly reduced. This filtering or smoothing allows the simulation to run with smaller N_c and N_D without increasing self-heating.

3.3. Accuracy condition

The accuracy condition $v_e \Delta t/\Delta x < 1$, where v_e is a characteristic velocity of the particles, ensures that particles with velocities less than or equal to v_e travel less than one cell per time step and thus sample the electric

field properly. Since electrons are much more mobile than ions, it is clear that if the electrons satisfy this condition, the ions also satisfy it. In Maxwellian plasmas, v_e is typically the electron thermal velocity, v_{te}. This implies that most of the electrons in the system satisfy the accuracy condition $v_{te}\Delta t/\Delta x < 1$, except for those electrons, on the tail of the electron energy distribution, whose velocities exceed the electron thermal velocity, v_{te}. This is particularly crucial in simulating RF discharges because the fast electrons in the tail of the distribution maintain the discharge; any inaccuracies in the fast electron population could have serious consequences. It is, however, clear that if the accuracy conditions $\omega_{pe}\Delta t < 0.2$ and $\Delta x/\lambda_{De} < 1$ are satisfied, $v_{te}\Delta t/\Delta x < 1$ is automatically satisfied since $v_{te} = \lambda_{De}\omega_{pe}$.

4. Explicit subcycling

Another inefficiency in conventional PIC-MCC is due to the difference in mass of ions and electrons. Ions are much heavier than electrons; they hardly move on the electron time scale and may be advanced with a much larger time step. This is the essence of electron-field advance and subcycling in particle simulations [40]. Electron subcycling improves the efficiency of multiple-species particle simulation by making the cost of advancing the ion negligible compared with that of the electrons. In electropositive discharges, where the ion population is roughly equal to the electron population, electron subcycling could at best save a factor of two in computing time by advancing the ions on a much larger time scale. In multiple-species particle simulation (such as simulation of electronegative discharges) where the ion population (including negative ions) is much larger than the electron population, a greater computational saving can be achieved with electron subcycling.

In the simplest explicit subcycling scheme, the electron plasma frequency sets the constraint on the time step for advancing the electrons and the electric field, $\omega_{pe}\Delta t_e < O(1)$, which is the smallest time scale in the system. The time steps for the ion species are set to ensure that the fastest ions still travel less than one cell per time step, $v_{ion_{max}}\Delta t_i/\Delta x < O(1)$. This could lead to choosing a large time step for the ions, $\Delta t_i \gg \Delta t_e$, in which case the ion density changes greatly every time the ions are advanced. This in turn causes a large displacement current at every ion-advance, which will appear as a pulse in the total-current and external-circuit current diagnostics. If these currents are calculated for purely diagnostic purposes and are not used as driving terms or boundary conditions in Maxwell's equations, the discharge physics does not seem to be affected. Although we see the pulses in our diagnostics when electron subcycling is used with explicit PIC, comparisons with conventional PIC simulations without subcycling reveals no noticeable differences.

Although we encountered a few limitations in discharge modelling with conventional PIC, many useful simulations both in discharges [23, 25–28, 41] and in many other plasma physics problems have been accomplished with a simple one-dimensional electrostatic code. Our next step is to extend the basic PIC-MCC techniques so that discharge simulations, over hundreds of RF cycles to reach discharge equilibrium, can be accomplished with far less computer time.

5. Direct implicit subcycling PIC simulation

Direct implicit particle simulation [42, 43] relaxes the $\omega_{pe}\Delta t$ time stability constraint and the $\Delta x/\lambda_{De} < 1$ accuracy constraint. As mentioned before, to obtain the proper physics in the simulation, Δt must then resolve the RF drive frequency ω_0, and Δx must resolve the sheath size at the boundary. In a driven RF discharge system, the time average sheath is $s \gg \lambda_{De}$, so Δx need not be very small.

The remaining constraint is the accuracy condition $v_{max}\Delta t/\Delta x < O(1)$ for the particles. This accuracy condition, as we saw before, is analogous to the Courant–Friedrichs–Lewy (CFL) stability condition for solution of finite-difference equations [36]. The fact that the orbits of the particles that violate this accuracy condition are poorly sampled could lead to numerical heating or cooling of these particles. In implicit particle simulation of discharges, for example, if the electrons on the tail of the energy distribution violate this accuracy condition, poor sampling of their orbits prevents them from reaching the ionization threshold. A multi-time scale scheme [44] can be used that allows fast electrons to move with a smaller time step, fulfilling the particle-CFL condition, while the majority of the electrons in the bulk plasma are pushed with a larger (implicit) time step. The computational overhead involved in maintaining and synchronizing several electron groups with different time steps caused us to abandon this method and to seek what improvements in computational efficiency could still be obtained while under the constraint of the particle-CFL condition. While multiple time scaling of the electrons is not used, subcycling of the electron-field solution, namely pushing the ions with a larger time step, is used in our simulations in both explicit and implicit versions.

5.1. Review of the algorithm

Before we describe the direct implicit subcycling method, we briefly illustrate a direct implicit advance for a single species of particles. The equations for a one-dimensional electrostatic model are

$$\dot{x} = v$$

$$\dot{v} = \frac{q}{m}E(x)$$

$$\partial_x^2\phi = -\rho/\varepsilon_0$$

$$E = -\partial_x\phi$$

where q and m are the particle's charge and mass

respectively. $E(x)$ is obtained by interpolating E from the grid to the particle located at x, and ρ is obtained by weighting particles back to the grid.

Implicit finite-difference versions of the particle advance equations are

$$x^n = x^{n-1} + \frac{\Delta t}{2}(v^n + v^{n-1}) \tag{5}$$

$$v^n = v^{n-1} + \frac{\Delta t}{2}\frac{q}{m}[E^n(x^n) + E^{n-1}(x^{n-1})]. \tag{6}$$

These equations are implicitly time-centred because x^n must be known to obtain E^n, but E^n must be known to advance x from time $(n-1)$ to n. A time-centred scheme is not the only choice. Other schemes, known as class C and class D, are well described in the literature [42, 45]. These schemes are also implicit and have various high-frequency damping and low-frequency accuracy properties. They also require storage of particle properties at multiple time steps. For our discharge modelling, we use the above time-centred implicit scheme for all particle species to avoid the extra storage and algorithmic complexity.

Following Langdon, Cohen, and Friedman [43], we combine equations (5) and (6) to obtain

$$x^n = \tilde{x}^n + \alpha E^n(x^n) \tag{7}$$

where $\alpha = (\Delta t/2)^2(q/m)$ and

$$\tilde{x}^n = x^{n-1} + \Delta t\, v^{n-1} + \alpha E^{n-1}(x^{n-1}). \tag{8}$$

After E^n is calculated, we find x^n and thus complete the implicit advance by the following approximation to equation (7):

$$x^n = \tilde{x}^n + \alpha E^n(\tilde{x}^n). \tag{9}$$

Note that a logistical problem with the implicit method is that E^n depends on ρ^n, which in turn depends on the particle locations x^n. Unfortunately, all the particle locations depend on E^n. One way to get around this problem is to linearize the locations x^n about $\tilde{x}^n$. Then ρ^n on the grid is written as

$$\rho^n = \tilde{\rho}^n + \delta\rho^n \tag{10}$$

where $\tilde{\rho}^n$ is found from interpolating particles at $\tilde{x}^n$ on to the grid and

$$\delta\rho^n = -\partial_x(\tilde{\rho}^n \delta x^n) \tag{11}$$

where $\delta x^n = \alpha E^n(x^n)$ from equation (7).

Equation (11) is derived by linearizing the particle-to-grid interpolation equation about $\tilde{x}^n$. Strictly speaking, δx^n is an individual quantity for each particle. To solve Poisson's equation, we use the approximation $\delta x^n \cong (\delta t/2)^2(q/m)E^n$ where E^n signifies the electric field at the grid point at which equation (11) is evaluated. After inserting the approximate definition of δx^n into equation (11), we insert the result into equation (10). Using equation (10) as the source term for Poisson's equation, and using definition $E^n = -\partial_x\phi^n$, we obtain the implicit Poisson equation

$$\partial_x[1 + \chi]\partial_x\phi = -\tilde{\rho}/\varepsilon_0 \tag{12}$$

where the n superscript is suppressed and

$$\chi \equiv (q\,\Delta t^2/4m\varepsilon_0)\tilde{\rho}.$$

For multiple species, the definitions of the terms $\tilde{\rho}$ and χ are generalized to

$$\tilde{\rho}_j = \sum_s q_s \sum_i W_j(\tilde{x}_i) \tag{13}$$

$$\chi_j = \sum_s (q_s^2\,\Delta t^2/2m_s\varepsilon_0) \sum_i W_j(\tilde{x}_i). \tag{14}$$

where q_s and m_s are the charge and mass of species s, $\tilde{x}$ is the portion of the position advance dependent on quantities known at time level $n-1$, and the W term indicates the weighting function used to interpolate from particles to the grid [13]. If each species is advanced with a different time step, Δt in equation (14) must be replaced by the species time step Δt_s, as we will discuss later.

The finite-difference version of equation (12) is

$$[1 + \chi_{j-1/2}]\phi_{j-1} - [2 + \chi_{j-1/2} + \chi_{j+1/2}]\phi_j + [1 + \chi_{j+1/2}]\phi_{j+1} = -\Delta x^2\tilde{\rho}_j/\varepsilon_0 \tag{15}$$

where $\chi_{j\pm1/2} = (\chi_j + \chi_{j\pm1})/2$, $j = 1, 2, \ldots, nc-2, nc-1$, and nc is the number of grid cells. In a voltage-driven RF discharge simulation, the left-hand plate is biased at the RF source voltage and the right-hand plate is referenced to zero potential. This gives $\phi_0 = V_{RF}(t)$ and $\phi_{nc} = 0$.

The electric field at the interior grid points can be determined by the finite-difference version of $E = -\partial_x\phi$,

$$E_j = (\phi_{j-1} - \phi_{j+1})/(2\,\Delta x). \tag{16}$$

At $j = 0$ and $j = nc$, an implicit Gauss law must be used to determine the field. An implicit Poisson equation can be written in vector notation as

$$\nabla\cdot(1 + \chi)\boldsymbol{E} = \tilde{\rho}/\varepsilon_0. \tag{17}$$

The integral representation of equation (17) produces the implicit Gauss law:

$$\int_S (1 + \chi)\boldsymbol{E}\cdot\mathbf{d}\boldsymbol{S} = Q/\varepsilon_0 \tag{18}$$

where Q, the appriximation to the enclosed charge, is due to $\tilde{\rho}$ and the surface charge density. Drawing a Gaussian pillbox for equation (18) around the left-hand wall and spanning the distance $j = -\frac{1}{2}$ to $j = \frac{1}{2}$ gives

$$[(1 + \chi)E]_{1/2} = \sigma_0/\varepsilon_0 + \tilde{\rho}_0\,\Delta x/2\varepsilon_0 \tag{19}$$

where σ_0 is the wall surface charge density. Inside the perfectly conducting wall, $E = 0$. At the wall, the Gauss law gives $E_0 = \sigma_0/\varepsilon_0$. Substituting this expression into equation (19) and solving for E_0 gives

$$E_0 = [(1 + \chi_{1/2})(\phi_0 - \phi_1)/\Delta x] - \tilde{\rho}_0\,\Delta x/2\varepsilon_0 \tag{20}$$

and similarly, for the right-hand wall,

$$E_{nc} = [(1 + \chi_{nc-1/2})(\phi_{nc-1} - \phi_{nc})/\Delta x] + \tilde{\rho}_{nc}\Delta x/2\varepsilon_0 \tag{21}$$

For a current-driven RF discharge simulation, the implicit boundary conditions are slightly different than for the explicit method [35] but can be easily worked out. Finally, it is assumed that, if $\tilde{x}$ penetrates the wall, then the particle's final location will be in the wall.

5.2. Implementation of direct implicit subcycling

The above procedure is used in combination with subcycling to form a direct implicit subcycling PIC method for simulating multiple-species plasmas. Here we will discuss an example of a plasma consisting of electrons and a single-ion species. The use of the direct implicit method alters the subcycling technique discussed before. The electrons are pushed with a small base time step Δt_e, and ions are pushed with a large time step Δt_i. During the calculation, a time interpolation of ion density is required. This interpolation causes the variation of the ion density to be continuous in time, significantly reducing the abrupt change in the displacement current as seen in the explicit subcycling. This time interpolation can also be used in explicit subcycling to avoid the discontinuities in displacement current.

Suppose $\Delta t_i = 4\,\Delta t_e$, where Δt_e is chosen to model the electrons accurately. The electrons are advanced in the time steps

$$n = 0, 1, 2, 3, 4, 5, 6, 7, 8, \ldots$$

The ions are advanced in the time steps

$$N = 0, 4, 8, \ldots$$

Both electrons and ions are moved with the direct implicit simulation technique for consistency. If electrons and ions were moved independently, the implicit corrections to the free stream densities would be as above

$$\delta\rho_e^n = -\partial_x[(q/4m)\tilde{\rho}_e^n \Delta t_e^2 E^n] \tag{22}$$

for the electrons and

$$\delta\rho_i^N = -\partial_x[(q/4m)\tilde{\rho}_i^N \Delta t_i^2 E^N] \tag{23}$$

for the ions.

The field must be calculated on the electron time scale (every Δt_e) with the Poisson equation

$$\partial_x^2\phi^n = -(\tilde{\rho}_e^n + \delta\rho_e^n + \tilde{\rho}_i^n + \delta\rho_i^n)/\varepsilon_0. \tag{24}$$

The key is to determine $\tilde{\rho}_i$ and $\delta\rho_i$ at the n time steps during which the ions are not pushed, for example 4 to 5 or 5 to 6. In these time steps, $\delta\rho_i$ retains the same form:

$$\delta\rho_i^n = -\partial_x[(q/4m)\tilde{\rho}_i^n \Delta t_i^2 E^n] \tag{25}$$

where we keep the same Δt_i as if we were actually pushing the ions from $t - \Delta t_i$ to t.

The approximation to $\tilde{\rho}_i$ for the time steps in which the ions are not pushed is given by linear weighting:

$$\tilde{\rho}_i^5 = (3/4)\tilde{\rho}_i^4 + (1/4)\tilde{\rho}_i^8 \tag{26}$$

$$\tilde{\rho}_i^6 = (2/4)\tilde{\rho}_i^4 + (2/4)\tilde{\rho}_i^8 \tag{27}$$

$$\tilde{\rho}_i^7 = (1/4)\tilde{\rho}_i^4 + (3/4)\tilde{\rho}_i^8. \tag{28}$$

Note that $\tilde{\rho}_i^{4,8}$ are due to actual free streaming of the ions. The implicit Poisson equation becomes

$$\partial_x[1 + \chi^n]\,\partial_x\phi^n = -(\tilde{\rho}_i^n + \tilde{\rho}_e^n)/\varepsilon_0 \tag{29}$$

where

$$\chi^n = (q/4m)(\Delta t_i^2\,\tilde{\rho}_i^n + \Delta t_e^2\,\tilde{\rho}_e^n).$$

Boundary conditions may be worked out from an implicit Gauss law based on the above equation.

The numerical procedure for moving the simulation from time step 4 to 8 is outlined below. The procedure is the same for moving the simulation from 8 to 12, 12 to 16, and so on.

(i) Pre-push the ions from 4 to 8.
(ii) Calculate $\tilde{\rho}_i$ for 5, 6, 7.
(iii) Pre-push the electrons from 4 to 5.
(iv) Field solve at 5.
(v) Post-push fast electrons from 4 to 5.
(vi) Repeat the electron steps for 5 to 6, 6 to 7, 7 to 8.
(vii) Post-push the ions from 4 to 8.

In the following section, we do a performance study comparing conventional and implicit PIC simulations for a generic RF discharge. The addition of subcycling improves computational efficiency by at most a factor of two since the example discharge is electropositive.

6. A performance study for a typical capacitive RF discharge

A performance study was done by Cohen *et al* [45] for class C and class D implicit algorithms applied to an expanding plasma slab problem. They started their simulation with a Maxwellian plasma at a given density and electron temperature, and the plasma slab was allowed to expand in the system. Their simulated system was isolated: no external heating mechanism was applied, and the total number of particles was held fixed. Thus, any change in the total energy of the system could only have originated in their numerical scheme. If the change in the total energy was positive, the system was considered to be numerically heated, and a negative change in the total energy was considered a numerical cooling.

We do a similar study for a generic RF discharge simulation. However, the simulated system is now much more complicated. Electrons and ions are constantly created in the system through ionization and lost from the system when they reach the electrodes. The RF power deposited into the system heats the particles. The electrons gain energy ohmically through the body of the plasma and stochastically by colliding with the oscillating sheaths, and lose energy through inelastic collisions with background neutral particles and by escaping from the system to the electrodes. The ions gain energy ohmically in the sheath, and carry off their energy when they reach the electrodes. The system reaches equilibrium when the particle loss rate equals the particle

generation rate, and when the power deposited into the system equals all the power losses.

6.1. Base model (prototype)

An RF discharge simulation run is brought to equilibrium with the conventional explicit PIC scheme. The system is a one-dimensional parallel plate argon RF discharge running with a current source of 2.56 mA cm^{-2} at 13.56 MHz. The system length is 2 cm, and the neutral gas pressure is 100 mTorr. (This is one of the cases studied and compared with Godyak's experimental results [3], which we will discuss in part II of this paper.) The plasma density in the bulk, obtained from the simulation, peaks at 8.7×10^9 cm^{-3}. The electron energy probability function (EEPF) is shown in figure 5. The EEPF can be represented as a sum of two Maxwellian distributions with temperatures of $T_l = 0.5$ eV and $T_h = 3$ eV, where T_l and T_h are the effective temperatures of the low- and high-energy electron groups. The corresponding electron thermal velocities associated with the low- and high-energy groups are $v_{te_l} = 4.4 \times 10^7$ cm s^{-1} and $v_{te_h} = 1.0 \times 10^8$ cm s^{-1}. The plasma frequency measured in the centre of the discharge peaks at $\omega_{pe} = 5.32 \times 10^9$ rad s^{-1}. We also have $\lambda_{De_l} = 0.00582$ cm as the electron Debye length associated with the low-energy group.

The time step Δt and the grid spacing Δx are chosen to resolve the electron plasma frequency accurately and the electron Debye length of the low energy electrons, $\omega_{pe}\Delta t < 0.2$ and $\Delta x/\lambda_{De} < 1$. This sets $\Delta t = 3.8 \times 10^{-11}$ s and the number of cells in the system to $N = 400$. The total number of electrons (or ions) in the system at equilibrium is roughly 35 000, which gives the number of electrons per Debye length to be $N_D \simeq 100$, and the number of electrons per cell to be $N_c \simeq 90$. The width of the driven sheath for this case is $s \simeq 0.6$ cm, which makes the actual length of the bulk discharge roughly half the system length. Thus, the actual values of N_D and N_c are larger in the bulk. The charge densities are digitally filtered [13] to reduce significantly numerical fluctuations and self-heating. The discharge reached equilibrium after several hundred RF cycles, at which time a restart file was created. Figure 6 shows the electron and ion heating rates ($J \cdot E$) at equilibrium. The electrons are heated strongly in the sheath region, while the overall electron heating rate in the bulk is very small. The ions are accelerated through the sheath by the time-averaged field in the sheath region. (The physics of these heating mechanisms will be investigated in part II.)

The discharge discussed above is used as our base case for purposes of comparison between conventional explicit and implicit subcycling PIC schemes. We start the simulation with the restart file described above with various time step sizes and grid cells. Since the simulation in each case is restarted from equilibrium, it only takes a few hundred RF cycles (which is the ion transit time for a thermal ion from the middle of the system to a wall for these parameters) before the system reaches a new equilibrium. In all cases, the power gained by ions stayed roughly the same, while the average kinetic energy of the electrons E_K changed. Each case was run for N_{RF} RF cycles (where $N_{RF} > 100$), after which the change in average kinetic energy of the electrons in the system ΔE_K was measured. Our concern in these comparisons is with both numerical heating and cooling of electrons which, as in Cohen *et al* [45], is measured as $(\Delta E_K/E_K)/N_{RF}$, the normalized change in average electron kinetic energy per RF cycle. Note that as ΔE_K approaches zero, energy conservation for electrons becomes roughly exact, but this does not guarantee the correct solution: the same average electron kinetic energy E_K can be obtained from different electron energy probability functions. Thus one must also pay careful attention to the EEPF.

Table 1 shows a summary of several cases studied

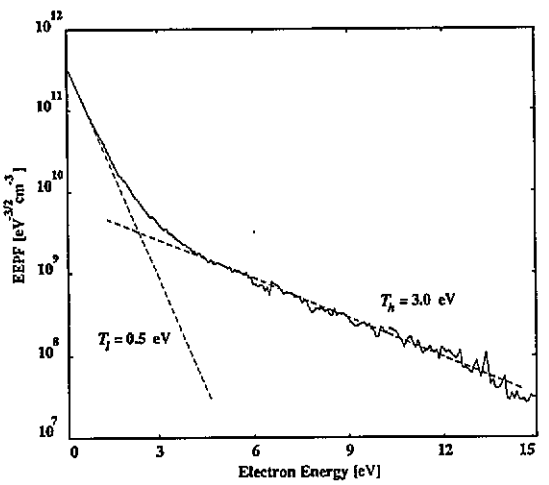

Figure 5. The electron energy probability function (EEPF) in a 2 cm gap current-driven RF discharge at the neutral pressure of 100 mTorr. The broken lines represent the two-temperature Maxwellian distribution of the discharge.

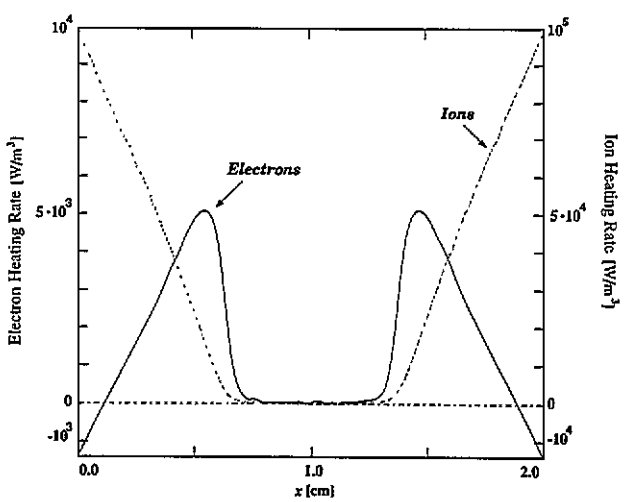

Figure 6. Electron and ion heating rates in the system at the neutral pressure of 100 mTorr, obtained with the conventional explicit PIC scheme.

Table 1. A comparison between conventional explicit and implicit subcycling PIC schemes. The parameter ω_{pe} is the electron plasma frequency; Δt_e is the time step with which the electrons are advanced; N is the number of grid cells in the system; N_c is the number of computer particles per cell; Δx is the numerical grid size; $\lambda_{De|}$ is the electron Debye length associated with the low-energy electrons; $v_{te|}$ is the electron thermal velocity associated with the high-energy electron group; V_{teh} is the electron thermal velocity associated with the high-energy electron group; k_{ion} is the ratio of ion to electron time steps. Each case was run for N_{RF} RF cycles (where $N_{RF} > 100$), after which the change in average kinetic energy of the electrons in the system ΔE_K was measured. The numerical heating/cooling rate is measured as $(\Delta E_K/E_K)/N_{RF}$, the normalized change in average electron kinetic energy per RF cycle. We also define the computing factor gained as a measure of how much CPU time is saved by using a larger time step size than in the base case. Cases 1–7 show results obtained using the explicit PIC scheme, while cases 8–16 are from the implicit subcycling scheme.

Case	$\omega_{pe}\Delta t_e$	N	N_c	$\Delta x/\lambda_{De\|}$	$v_{te\|}\frac{\Delta t_e}{\Delta x}$	$v_{teh}\frac{\Delta t_e}{\Delta x}$	k_{ion}	$\frac{\Delta E_K/E_K}{N_{RF}}$	Factor
1	0.2	50	700	6.87	0.041	0.090	1	0.000000	1
2	0.2	150	233	2.29	0.123	0.280	1	0.000232	1
3	1.0	50	700	6.87	0.202	0.460	1	0.000262	5
4	1.0	100	350	3.43	0.409	0.930	1	0.000397	5
5	2.0	50	700	6.87	0.409	0.930	1	0.001000	10
6	2.0	100	350	3.43	0.823	1.870	1	0.003124	10
7	2.0	200	175	1.72	1.641	3.730	1	unstable	10
8	0.2	50	700	6.87	0.041	0.090	1	0.000000	1
9	0.2	150	233	2.29	0.123	0.280	1	0.000112	1
10	1.0	50	700	6.87	0.202	0.460	1	0.000000	5
11	1.0	50	700	6.87	0.202	0.460	10	0.000000	10
12	1.0	100	350	3.43	0.409	0.930	1	0.000225	5
13	2.0	50	700	6.87	0.409	0.930	1	−0.000179	10
14	2.0	100	350	3.43	0.823	1.870	1	−0.001244	10
15	2.0	200	175	1.85	1.641	3.730	1	0.001665	10
16	2.0	400	88	0.85	3.282	7.460	1	0.008397	10

over a wide range of chosen numerical parameters with both schemes. Cases 1–7 are obtained with the explicit PIC scheme, while cases 8–16 are obtained with the implicit subcycling scheme. The parameter k_{ion} is the ratio of ion to electron time steps. Electron subcycling is achieved when k_{ion} is larger than one.

6.2. Explicit PIC

Case 1 in table 1 is identical to the base case, except for a smaller number of cells and lack of digital smoothing. In a sense, decreasing the number of cells is equivalent to smoothing the charge densities because smoothing reduces the short wavelength numerical fluctuations in the system. Note that $\lambda_{De_|}$ is rather poorly resolved by the grid. Nonetheless, for $\omega_{pe}\Delta t = 0.2$, the particle-CFL condition is well satisfied for high-energy electrons as well as for low-energy electrons by using 50 grid points, enough to resolve the driven RF sheath length. After about 100 RF cycles, the energy conservation remained very nearly exact and the EEPF remained the same as the base case.

Cases 2–7 in table 1 are attempts at using larger time step sizes with the explicit scheme in order to gain computational efficiency. Notice that as the time step Δt is raised, the particle-CFL accuracy condition $v_{te}\Delta t/\Delta x < 1$ for both groups of particles demands a larger number of cells in the system. Because no digital smoothing is used, electron self-heating increases as the number of cells is increased. Figure 7 shows spatial electron heating rates ($J \cdot E$) for cases 1, 5, and 6. The excess heating rate in the bulk for cases 5 and 6 is due to self-heating of the slow electron group. Note that in cases 5 and 6, the particle-CFL accuracy condition is not satisfied for the high-energy electron group. This means that most of the fast electrons travel more than one cell

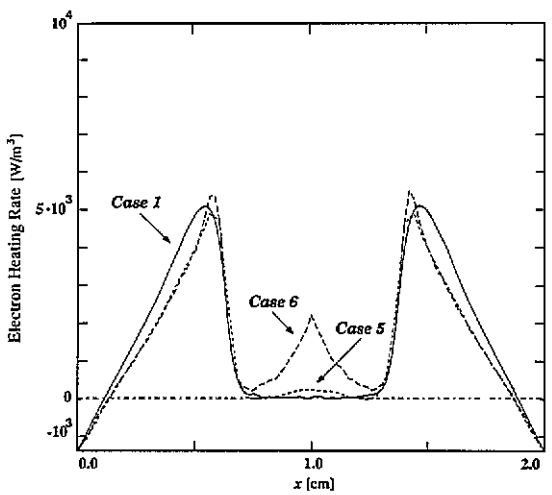

Figure 7. Electron heating rates for cases 1, 5, and 6 shown in table 1. The excess electron heating in the bulk for cases 5 and 6 (where $\omega_{pe}\Delta t = 2$) is due to the self-heating of the low-energy electrons in the bulk.

per time step and do not sample the RF field in the sheath regions properly, which accounts for lower heating rates in the sheaths. Over a few hundred RF cycles, excess numerical heating in the bulk leads to a higher effective electron temperature for the low-energy group, as seen in figure 8. The power deposited in the system for all cases 2–7 remains roughly the same as the base case, while the plasma density measured in the middle of the system for cases 2–7 is lower than the density for the base case. The lower plasma density can be explained by the power balance in equation (3). Taking the ion loss rate from the bulk plasma to be the ion sound speed, $u_B = (kT_e/M)^{1/2}$, we can see that the higher bulk electron temperature gives a higher loss rate, while the generatio n rate, which is determined mostly by the effective temperature of the fast electrons, remains almost the same. It is clear from equation (3) that, for a fixed power, as the electron temperature increases, the plasma density decreases.

Attempting to increase the number of cells in the system leads to instabilities when $\omega_{pe}\Delta t \geqslant 2$ and $v_{te_i}\Delta t/\Delta x > 1$. This is shown as case 7 in table 1.

6.3. Implicit subcycling

The second part of table 1 outlines cases 8–16 which are studied with the implicit subcycling PIC scheme. The parameters chosen in case 8 are the same as case 1 and identical results are obtained. However, the time to run the same number of RF cycles with the implicit scheme increases by roughly 40%, because the scheme requires a more complex particle advancing routine. We define the computing factor gained as a measure of how much CPU time is saved by using a larger time step size than in the base case. In explicit PIC scheme, doubling, Δt gains a factor of two in computational efficiency. However, doubling Δt does not translate into a computing factor of two in the implicit scheme because of the more complex particle advance. Note that, in all the explicit cases, a computing factor of roughly two could be gained through electron subcycling.

The parameters in cases 13 and 14 are the same as 5 and 6 discussed above. Figure 9 shows the electron heating rates for cases 1, 13, and 14. Numerical heating of the low-energy electrons in the bulk in cases 13 and 14 is seen to be very small. However, the sheath heating of the electrons is much smaller relative to the base case because the particle-CFL accuracy condition is violated by the high-energy electron group. Thus the effective temperature of the high-energy electrons decreases, and the fast electrons are said to be numerically cooled, as seen in figure 10. Because the numerical cooling of the high-energy electrons is much larger than the self-heating of the low-energy electrons, the overall numerical

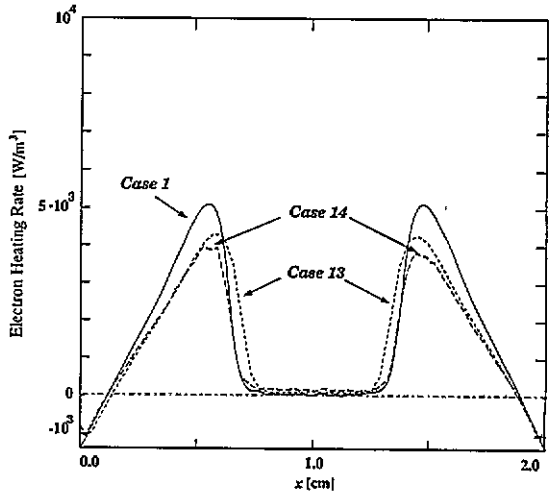

Figure 9. The electron heating rates for cases 1, 13, and 14 shown in table 1. No significant numerical heating is observed in the bulk for cases 13 and 14 (where $\omega_{pe}\Delta t = 2$), but the sheath heating of the electrons is much smaller.

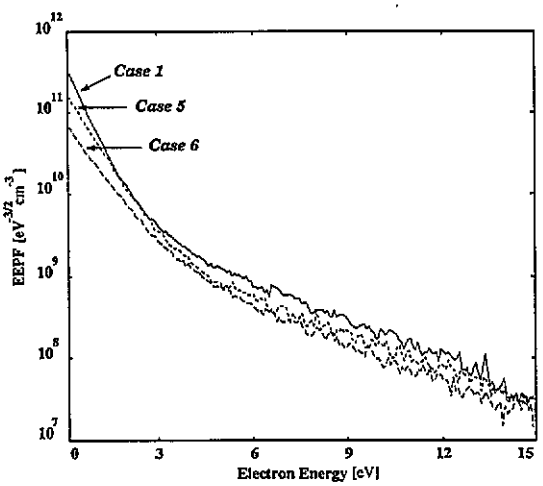

Figure 8. The electron energy probability functions (EEPF) at the neutral pressure of 100 mTorr for cases 1, 5, and 6 shown in table 1. The numerical heating in the bulk causes the effective temperature of the low-energy electrons to increase.

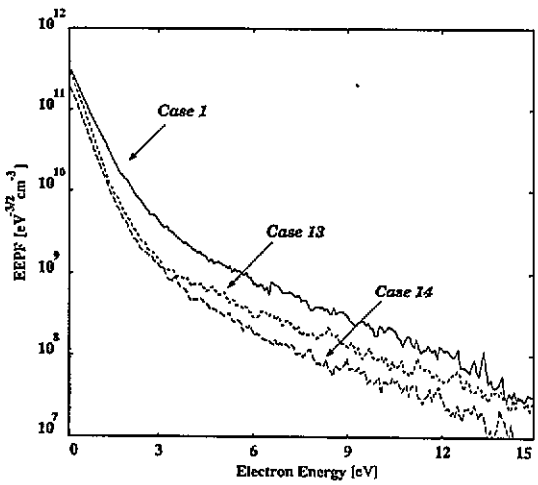

Figure 10. The electron energy probability functions (EEPF) at the neutral pressure of 100 mTorr for cases 1, 13, and 14 shown in table 1. The numerical cooling of the high-energy electrons causes the effective temperature of the high-energy group to decrease.

effect is cooling for cases 13 and 14. Note that, since the ionization rate is a strong function of the electron temperature, this numerical cooling causes the ionization (generation) rate to drop, which in turn decreases the plasma density. The integrated area below the EEPF is proportional to the electron density. Figure 10 shows smaller densities for cases 13 and 14. It is therefore desirable to maintain $v_{te_h} \Delta t/\Delta x < 0.5$.

A similar conclusion was reached by Cohen *et al* [45]. They found that for $v_{te} \Delta t/\Delta x < 0.3$, energy conservation was roughly exact for a single-temperature Maxwellian energy distribution. The best cases presented here are 10 and 11, where no noticeable numerical heating or cooling is observed. The difference between the two cases is that the electron subcycling used in case 11 gains another factor of two in computational efficiency. Because the time step size in case 11 is five times larger than the base case, the computing factor gained in this case is slightly less than an order of magnitude. Figures 11 and 12 show an excellent agreement of the

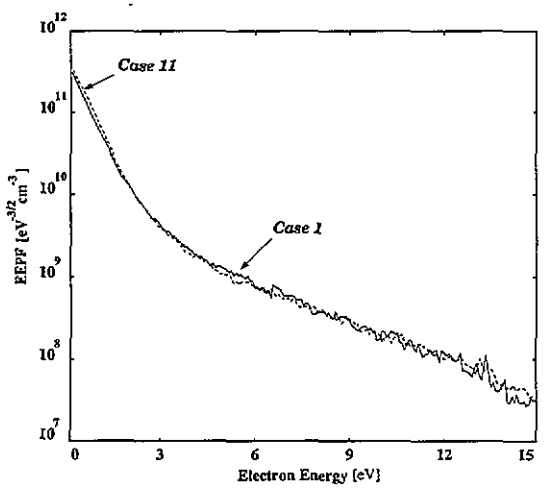

Figure 11. The electron energy probability functions (EEPF) at the neutral pressure of 100 mTorr for cases 1 and 11 shown in table 1.

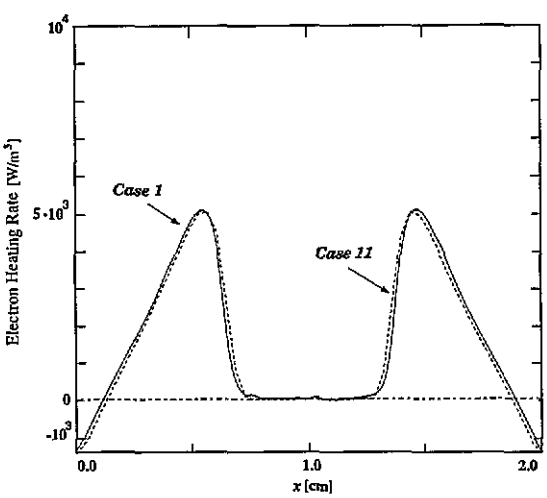

Figure 12. The electron heating rates for cases 1 and 11 shown in table 1.

EEPF and electron heating rate between the base case and case 11. A larger computing factor could be gained if we decrease the number of cells in the system to less than 50, or if we increase the length of the simulated system.

7. Conclusion

Particle-in-cell Monte Carlo simulation has become a very effective tool in exploring processing plasmas and in particular capacitive RF discharges. We discussed conventional PIC simulation and its limitations in terms of computational efficiency, reviewed the implicit subcycling method used to improve computational efficiency, and compared the performances of conventional and implicit subcycling PIC simulation for our RF discharge model. The implicit subcycling scheme resulted in an order of magnitude reduction in the simulation run time when accuracy conditions were satisfied. These algorithms were incorporated into our bounded one-dimensional electrostatics code, PDP1.

The physical length of our prototype RF discharge model was chosen to be the same as that in Godyak's experiment [1, 3], for the comparison presented in part II. The factor gained in computational efficiency can be increased for longer systems, which can be seen from the accuracy condition $v_{te_h} \Delta t/\Delta x < 0.5$. The grid spacing Δx must resolve the time-averaged RF sheath width s, that is $\Delta x/s < 0.2$. This sets a rough limit on the maximum grid spacing, and through the accuracy condition, we obtain an upper limit on the time step to be $\Delta t < 0.1 s/v_{te_h}$. The time step must also resolve the RF period $2\pi/\omega_0$.

Acknowledgment

This work was performed with support in part from the Lawrence Livermore National Laboratory under USA Department of Energy Contract W-7405-ENG-48. The portion of the work performed at Berkeley was supported by the National Science Foundation under Grant ECS-8910827, USA Department of Energy Contract DE-FG03-90ER54079, and Office of Naval Research Contract FD-N00014-90-J-1198. Discussions with Dr Alex Friedman, Dr Richard Procassini, Dr Ron Cohen and Dr Dennis Hewett of Lawrence Livermore National Laboratories are gratefully acknowledged.

References

[1] Godyak V A and Piejak R B 1990 *Phys. Rev. Lett.* **65** 996
[2] Godyak V A, Piejak R B and Alexandrovich B M 1991 *IEEE Trans. Plasma Sci.* **19** 660
[3] Godyak V A, Piejak R B and Alexandrovich B M 1992 *Plasma Sources Sci. Technol.* **1** 36
[4] Kobayashi K, Mutsukura N and Machi Y 1990 *J. Appl. Phys.* **68** 2657
[5] Wood B P, Lieberman M A and Lichtenberg A J 1991 *IEEE Trans. Plasma Sci.* **19** 619

[6] Godyak V A and Sternberg N 1990 *Phys. Rev.* A **42** 2299
[7] Misium G R, Lichtenberg A J and Lieberman M A 1989 *J. Vac. Sci. Technol.* A **7** 3
[8] Lieberman M A 1988 *IEEE Trans. Plasma Sci.* **16** 638
[9] Graves D B and Jensen K F 1986 *IEEE Trans. Plasma Sci.* **14** 78
[10] Boeuf J P 1987 *Phys. Rev.* A **36** 2782
[11] Gogolides E, Nicolai J P and Sawin H H 1989 *J. Vac. Sci. Technol.* A **7** 1001
[12] Meyyappan M and Govindan T R 1991 *IEEE Trans. Plasma Sci.* **19** 122
[13] Birdsall C K and Langdon A B 1991 *Plasma Physics Via Computer Simulation* (Bristol: Adam Hilger)
[14] Hockney R W and Eastwood J W 1988 *Computer Simulation Using Particles* (Bristol: Adam Hilger)
[15] Procassini R J 1990 *Kinetic Particle-in-Cell Simulations of Transport in a Tokamak Scrape-off Layer, PhD Thesis* University of California, Berkeley, CA ch 4
[16] Hunter S R 1977 *Aust. J. Phys.* **30** 83
[17] Boeuf J P and Marode E 1982 *J. Phys. D: Appl. Phys.* **15** 2169
[18] Kushner M J 1985 *J. Appl. Phys.* **58** 4024
[19] Kushner M J 1983 *J. Appl. Phys.* **54** 4958
[20] Thompson B E, Sawin H H and Fisher D A 1988 *J. Appl. Phys.* **63** 2241
[21] Kaufman Y 1988 *J. Phys. D: Appl. Phys.* **21** 442
[22] Lin S L and Bardsley J N 1977 *J. Chem. Phys.* **66** 435
[23] Surendra M, Graves D B and Morey I J 1990 *Appl. Phys. Lett.* **56** 1022
[24] Birdsall C K 1991 *IEEE Trans. Plasma Sci.* **19** 65
[25] Vender D and Boswell R W 1990 *IEEE Trans. Plasma Sci.* **18** 725
[26] Surendra M and Graves D B 1991 *IEEE Trans. Plasma Sci.* **19** 144
[27] Vahedi V, Lieberman M A, Alves M V, Verboncoeur J P and Birdsall C K 1991 *J. Appl. Phys.* **69** 2008
[28] Alves M A, Lieberman M A, Vahedi V and Birdsall C K 1991 *J. Appl. Phys.* **69** 3823
[29] Turner M M and Hopkins H B 1992 *Phys. Rev. Lett.* **69** 3511
[30] Boeuf J P and Pitchford L C 1991 *IEEE Trans. Plasma Sci.* **19** 286
[31] Sato N and Tagashira H 1991 *IEEE Trans. Plasma Sci.* **19** 102
[32] Sommerer T J and Kushner M J 1992 *J. Appl. Phys.* **71** 1654
[33] Vahedi V 1993 *Modelling and Simulation of* RF *Discharges Used For Plasma Processing, PhD Dissertation* University of California, Berkeley, CA
[34] Lawson W S 1989 *J. Comput. Phys.* **80** 253
[35] Verboncoeur J P, Alves M A, Vahedi V and Birdsall C K 1993 *J. Comput. Phys.* **104** 321
[36] Sod G A 1985 *Numerical Methods in Fluid Dynamics* (Cambridge: Cambridge University Press)
[37] Surendra M, Graves D B and Jellum G M 1990 *Phys. Rev.* A **41** 1012
[38] Cramer W H 1959 *J. Chem. Phys.* **30** 641
[39] Hockney R W 1971 *J. Comput. Phys.* **8** 19
[40] Adam J C, Gourdin-Serveniere A and Langdon A B 1982 *J. Comput. Phys.* **47** 229
[41] Vahedi V, DiPeso G, Leiberman M A, Rognlien T D and Birdsall C K 1993 *Phys. Fluids* B **5** 2719
[42] Cohen B I, Langdon A B and Friedman A 1982 *J. Comput. Phys.* **46** 15
[43] Langdon A B, Cohen B I and Friedman A 1983 *J. Comput. Phys.* **51** 107
[44] Friedman A, Parker S E, Ray S L and Birdsall C K 1991 *J. Comput. Phys.* **96** 54
[45] Cohen B I, Langdon A B, Hewett D W and Procassini R J 1989 *J. Comput. Phys.* **81** 151